Talanta 122 (2014) 166–171

Contents lists available at ScienceDirect

Talanta

journal homepage: www.elsevier.com/locate/talanta

SPR bacterial pathogen biosensor: The importance of fluidic conditions and probing depth

Chun Jen Huang [a], Wolfgang Knoll [b], Angela Sessitsch [c], Jakub Dostalek [b,*]

[a] Graduate Institute of BioMedical Engineering, National Central University, (32001) No. 300, Jhongda Rd., Jhongli City, Taoyuan County 320, Taiwan
[b] AIT – Austrian Institute of Technology, BioSensor Technologies, Muthgasse 11, 1190 Vienna, Austria
[c] AIT Austrian Institute of Technology, Bioresources Unit, Konrad-Lorenz-straße 24, 3430 Tulln, Austria

ARTICLE INFO

Article history:
Received 12 September 2013
Received in revised form
13 January 2014
Accepted 20 January 2014
Available online 31 January 2014

Keywords:
Biosensor
Surface plasmon resonance
Long range surface plasmon
Bacterial pathogen
Shear stress
Diffusion limited mass transfer

ABSTRACT

The sensitivity of surface plasmon resonance (SPR) biosensor technology for detection of bacterial analytes is investigated as a function of (a) sample flow conditions and (b) depth of probing electromagnetic field. These parameters are extremely important as such analytes exhibit large (of around micrometer) size which significantly hinders their diffusion-driven transfer from a liquid sample to the sensor and their subsequent specific capture by attached recognition elements. This is due to small diffusion coefficient and strong shear stress that decreases the stability of bonds between the bacterium specific epitope and recognition elements immobilized at the sensor surface. The importance of accurate control of sample flow conditions and probing depth in order to maximize SPR sensor response is experimentally demonstrated and supported by an analytical theory. The tuning of the probing depth of surface plasmon evanescent field to match the size of the target analyte is pursued by using long range surface plasmons.

1. Introduction

Surface plasmon resonance (SPR) biosensor technology offers the advantage of label-free and real-time detection method that become increasingly exploited for an analysis of chemical and biological species [1]. In SPR biosensors, a liquid sample with a target analyte is flowed over the sensor surface with attached recognition elements. The capture of target analyte on the surface is associated with an increase in the refractive index that is probed by resonantly excited surface plasmons. In important application areas including food control and medical diagnostics, SPR biosensors hold potential for simpler and faster detection of bacterial pathogens which are currently routinely analyzed by time-consuming laboratory-based methods such as culturing [2], polymerase chain reaction [3], and enzyme-linked immunosorbent assays. Up to now, SPR biosensors were implemented for detection of a range of bacterial pathogens including *Escherichia coli* (*E. coli*) O157:H7 [4–6], *Salmonella* [7], and *Listeria monocytogenes* [7,8] and they were shown to detect these analytes at concentrations between 10^3 and 10^7 colony forming unit (cfu) per mL. However, this sensitivity is not sufficient as for many common pathogens even several cells in a sample can be infective [9]. The sensitivity of bacterial pathogen SPR biosensors is mainly impeded by low capture efficiency and by small refractive index changes that are associated with the binding of bacterial cell on the sensor surface. Due to micrometer size of bacterial pathogens, the mass transfer of such analyte from analyzed liquid sample to the sensor surface is strongly hindered by slow diffusion. Moreover, the captured cells are exposed to a shear stress which destabilizes their bonds with catcher molecules [10–12]. In addition, regular SPR biosensors typically probe the sensor surface with surface plasmon field that evanescently decays to distances between 100 and 200 nm from the surface. Therefore, only a small portion of adhered bacteria is probed and contributes to measured optical signal.

Various approaches have been investigated in order to advance the performance of bacterial pathogen SPR biosensors. These include analyte pre-concentration by magnetic particles [13], dielectrophoresis [14,15], and by disrupting bacterial analyte [16]. In addition, assays with an amplification of small refractive index changes induced by the binding of bacterial pathogens (refractive index of bacteria of 1.38 [17] is very close to that of aqueous samples 1.33) were developed by using nanoparticle labels [18]. Only recently, a layer architecture that supports long range surface plasmons (LRSPs) was reported for the SPR detection of bacterial pathogens [18–22]. These surface plasmon modes originate from the coupling of two SPs on opposite surfaces of a thin metallic film that is embedded between two dielectrics with similar refractive indices. LRSPs exhibit more extended profile of

* Corresponding author. Tel.: +43 50550 4308.
E-mail address: jakub.dostalek@ait.ac.at (J. Dostalek).

0039-9140/$ - see front matter © 2014 Elsevier B.V. All rights reserved.
http://dx.doi.org/10.1016/j.talanta.2014.01.022

evanescent field that can be tuned to overlap with large bacterial pathogens. Moreover, LRSPs exhibit smaller losses than regular SPs which improves the figure of merit of SPR measurements and allowed for the implementing of high resolution SPR biosensors [23]. This paper explores possibilities of maximizing SPR biosensor response due to the capture of bacterial analyte by tuning the flow-conditions and profile of electromagnetic field of surface plasmon waves. The affinity binding of model (non-harmful) bacteria *E. coli* K12 to the surface functionalized with specific antibodies was observed *in situ* and the sensitivity of SPR biosensor platforms with regular SPs and LRSPs is compared for diffusion mass transfer-limited and a shear stress-limited regimes. To best of our knowledge, detail investigation on how these parameters affect the sensitivity of SPR biosensors for detection of bacterial pathogens was not reported up to now and we believe that the presented results can provide valuable leads for future development of bacterial pathogen SPR biosensors with improved sensitivity.

2. Materials and methods

2.1. Chemicals and reagents

Goat polyclonal immunoglobulin G antibody (positive control IgG, p-IgG) reacting with O and K antigenic serotypes of *E. coli* was purchased from Abcam (cat. no. ab13627, Cambridge, UK). Goat polyclonal IgG (negative control IgG, n-IgG) to *E. coli* O157:H7 was obtained from KPL, Inc. (cat. no. 01-95-90, Gaithersburg, MD). The antibody against *E. coli* O157:H7 does not recognize *E. coli* K12 epitopes and was used in a control experiment. Dithiolaromatic PEG3 (PEG-thiol) and dithiolaromatic PEG6-carboxylate (COOH-thiol) were from SensoPath (Bozeman, MT). 1-ethyl-3-(3-dimethylamino-propyl) carbodiimide (EDC) and N-hydroxysulfosuccinimide (NHS) were bought from Pierce (Rockford, IL). Sodium acetate, acetic acid, Tween 20 and absolute ethanol (grade:200PR) were from Sigma-Aldrich (Schnelldorf, Germany). Phosphate buffered saline (PBS, 140 mM NaCl, 10 mM phosphate, 3 mM KCl, and a pH of 7.4) was acquired from Calbiochem (Darmstadt, Germany). 20 mM acetate buffer (ACT) was prepared from sodium acetate and its pH was adjusted by titrating with acetic acid to pH 5.5. In order to suppress non-specific adsorption, PBS was spiked with Tween 20 at 0.05% volume concentration (PBST). Hellmanex II and LaSFN9 glass substrates were acquired from Hellma Optik (Jena, Germany). Cytop (CTL-809M, 9 wt% in the solvent of CT-solv 180) was obtained from Asahi Glass (Tokyo, Japan).

2.2. Optical setup

An optical setup for the excitation of LRSPs by using attenuated total reflection (ATR) method with Kretschmann geometry was used as described previously [24]. As shown in Fig. 1a, TM-polarized beam emitted by a He–Ne laser (PL610P, Polytec, Germany, power 2 mM, wavelength $\lambda = 632.8$ nm) was coupled to 90° LASFN9 optical prism. A sensor chip with a layer structure supporting LRSPs or regular SPs was optically matched to the prism base by using refractive index matching oil (Cargille, USA). The resonant excitation of SPs or LRSPs was controlled by using a rotation stage (Hans Huber AG, Germany). The intensity of the reflected light beam was detected by using a photodiode connected to a lock-in amplifier (Model 5210, Princeton Applied Research, USA) with the standard deviation of $\sigma_R = 8 \times 10^{-4}$. The reflectivity R was measured as a function of angle of incidence θ or time t. For the time-resolved measurements, the angle of incidence θ was set below the resonant angle in the region where the slope of the angular reflectivity $dR/d\theta$ was maximum. The data acquisition and analysis were performed by using software Wasplas and Winspall, respectively, developed at the Max Planck Institute for Polymer Research (Mainz, Germany). Sensor chips with LRSP and SP-supporting layer structures were prepared on a LASFN9 glass slide. For the excitation of SPs, 46 nm thick gold layer was deposited on a glass substrate by using magnetron sputtering (UNIVEX 450C from Leybold Systems, Germany). As a LRSP-supporting layer structure, a Cytop layer was deposited by spin-coating followed by the sputtering of a thin gold layer as described

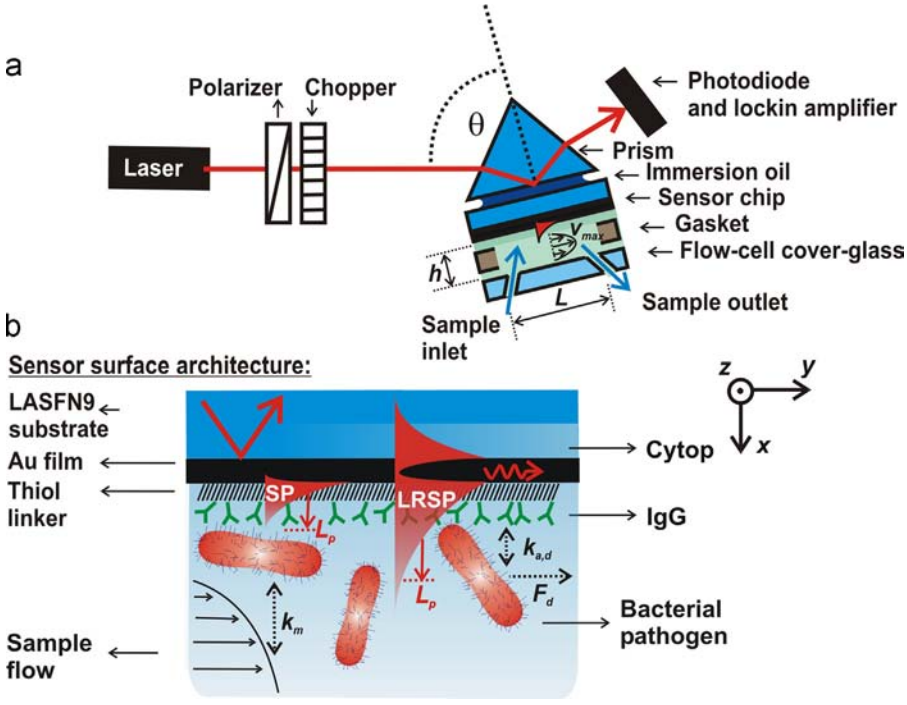

Fig. 1. Schematics of (a) optical setup (b) sensor chip layer architecture supporting LRSP with antibody recognition elements for a capture of target analyte.

in our previous publication [25]. The thickness of gold and Cytop layers was determined by AFM (Agilent Technologies, CA) and a surface profiler (Alpha-step IQ, KLA Tencor, CA) as 15.75 ± 0.26 nm and 887 ± 11 nm, respectively (error denotes the standard deviation).

2.3. Fluidic conditions

A flow cell was attached on the sensor chip in order to flow liquid samples. The flow rate was controlled by a peristaltic pump (Reglo, Ismatec, Switzerland) that was connected to a flow cell by using rubber tubing (Tygon R3607, Ismatec, Switzerland). The flow chamber was fabricated by casting a photolithographically defined relief into polydimethylsiloxane (PDMS). The depth of the flow chamber was $h=95$ μm, length $L=9$ mm and width $w=6$ mm, see Fig. 1. The volumetric flow rate between 50 μL min^{-1} and 700 μL min^{-1} was used which corresponds to the Reynolds number between $Re=8.8$ and 123 and Peclét number between $Pe=138$ and 1927, respectively. Therefore, the flow in a flow chamber was laminar and the flow distribution $v_y(x)$ across the flow channel exhibited parabolic profile with the maximum flow velocity v_{max} in the middle of the cell ($x=h/2$) and $v=0$ at the sensor surface ($x=0$). Let us note that the used Cartesian coordinates x,y, and z are defined as shown in Fig. 1b.

2.4. Functionalization of the sensor chip

PEG-thiol and COOH-thiol were dissolved in ethanol that was purged with argon at a molar ratio of 9:1 with a total thiol concentration of 0.2 mM. After the deposition of a gold layer, sensor chips were immediately soaked in the thiol solution and stored under argon atmosphere for at least 24 h in order to form a well ordered mixed self-assembled monolayer (SAM). Afterwards, their surface was rinsed with ethanol, dried in a stream of nitrogen, and *in situ* modified by IgG against *E. coli* K12 or O157:H7 as further described. Firstly, aqueous solution with EDC and NHS at the concentrations of 0.4 M and 0.1 M, respectively, was flowed for 20 min over the sensor surface with mixed thiol SAM in order to convert carboxylic moieties to active esters. Afterwards, ACT solution with IgG molecules dissolved at a concentration of 50 μg mL^{-1} was flowed through the flow cell for 50 min in order to anchor antibodies through reacting their amine groups with active ester-activated carboxylic groups. Finally, 1 M ethanolamine hydrochloride solution was flowed through the flow cell for 20 min in order to passivate unreacted active ester groups followed by rinsing with PBST buffer until a stable baseline was established in the sensor response $R(t)$.

2.5. Sample preparation, characterization and detection assay

E. coli K12 was cultured overnight in tryptic soy broth with aeration at 37 °C. Then, 10 mL bacteria liquid culture was removed and centrifuged at 2000*g* for 10 min at 4 °C followed by a removal of the supernatant. The pellet was washed twice with PBS buffer and re-suspended in 10 mL PBST buffer, aliquoted and stored at 4 °C prior to the analysis. The cell concentration was determined by using a conventional colony counting method. Briefly, a sample with cells was cultured on agar plates for four days followed by the counting of viable colonies. The average hydrodynamic diameter of *E. coli* in PBST was determined by dynamic light scattering as $a=1.57$ μm (Zetasizer from Malvern Instruments, Worcestershire, UK). For the SPR biosensor experiment, samples with *E. coli* K12 diluted at concentrations between 10^4 cfu mL^{-1} and 10^8 cfu mL^{-1} were prepared and sequentially injected to the sensor. After the flow of each sample, the sensor surface was rinsed with PBST buffer until a baseline was established. For calibration, the surface density of captured *E. coli* K12 cells was determined by an optical microscope (Hund Wetzlar, Germany) on the same sensor chip with attached flow cell as used in SPR experiments. The images were recorded with a time interval of 30 s and number of captured bacteria was evaluated by using ImageJ software (National Institutes of Health, USA).

2.6. Affinity binding of bacterial pathogens to the sensor surface

Upon a flow of an aqueous sample through SPR biosensor flow cell, dissolved bacterial pathogens can reach its surface with attached recognition elements via diffusion across an unstirred layer. The analyte diffusion mass transfer rate from the solution to the surface can be described by using a two-compartment model as [26]:

$$k_m = 1.378\left(\frac{v_{max}{D_s}^2}{hL}\right)^{1/3}, \quad (1)$$

where D_s is a diffusion coefficient of an analyte in the liquid sample. For the used bacterium analyte, $D_s=2.8\times10^{-7}$ mm^2 s^{-1} was determined by dynamic light scattering. Let us note that Eq. (1) is valid for the laminar flow in the flow cell and that it neglects diffusion parallel to the sensor surface. These assumptions hold as Reynolds number $Re<2300$ and Peclét number is $Pe\gg1$ (see Section 2.3). As Fig. 1b illustrates, a shear stress parallel to the surface acts on captured analyte upon a flow of a sample. It is caused by a drag force F_d and it destabilizes bonds between the antibodies and specific membrane epitope of captured bacteria. This force is proportional to the maximum sample flow velocity v_{max} and can be expressed as:

$$F_d = 32a\eta\frac{dv_y}{dx} = 1.28\times10^2 a\eta\frac{v_{max}}{h}, \quad (2)$$

where a is the hydrodynamic radius of a bacteria and η is the viscosity of a sample. As the size of bacterial pathogen a is orders of magnitude larger than that of used IgG antibody recognition elements, multiple antibodies can bind to a captured bacterium. Such multiple point attachment can be described by numerous models [12] and it exhibits more complex nature than that typically observed for the binding of smaller biomolecules [10]. The destabilization of bonds between a cell and a surface with recognition elements can be described by dissociation affinity binding rate k_d as the following function of the drag force F_d:

$$k_d = k_d^0\exp(\gamma F_d/k_bT), \quad (3)$$

where k_d^0 is the dissociation rate constant for $v_{max}=0$, k_b is the Boltzmann constant, T is the temperature, and γ is a characteristic length of the interaction between receptors tethered to the surface and bacterium epitope on the cell membrane. There can be shown that for large flow velocities v_{max}, the equilibrium surface density of captured bacteria on the surface is proportional to $1/k_d$ (average time upon which the analyte stays captured on the surface). Let us note that this simplified model omits other phenomena related to the multiple point attachment and shear stress (*e.g.*, rolling of cells along the surface [12]).

3. Results and discussion

3.1. Characteristics of the sensor surface probed by LRSP and SP modes

Angular reflectivity spectra $R(\theta)$ shown in Fig. 2a were measured for the probing of the sensor surface with regular SPs and LRSPs. The excitation of these modes is manifested as a sharp dip in reflectivity spectrum with the full width of half maximum

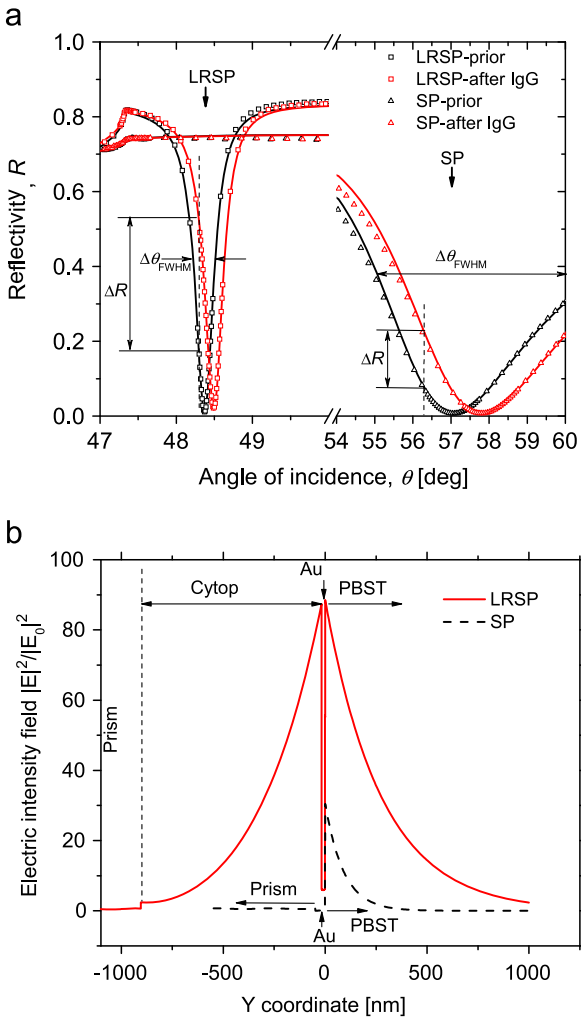

Fig. 2. (a) Angular reflectivity spectra measured for the layer architecture supporting LRSPs (squares) and regular SPs (triangles). Measurements were performed in PBST before (in black) and after (in red) immobilization of IgG antibody recognition elements. Corresponding fitted curves are indicated (lines). (b) Simulated profile of electric intensity field upon the resonant excitation of LRSPs (red solid curve) and regular SPs (black dashed curve). (For interpretation of the references to color in this figure legend, the reader is referred to the web version of this article.)

(FWHM) of $\Delta\theta_{FWHM}=4\pm0.11^\circ$ for SPs and $\Delta\theta_{FWHM}=0.3\pm0.01^\circ$ for LRSPs. It should be noted that the narrower resonance associated with the excitation of LRSPs allows for more accurate measurements of refractive index changes on the sensor surface and thus for more precise readout of assays. As reported in our previous study [24], the figure of merit for the used LRSP-supporting structure is of about four-fold larger compared to that on which regular SPs propagate when detecting (bulk) refractive index changes within the whole evanescent field of these waves. Measured curves $R(\theta)$ were fitted by a Fresnel reflectivity-based model in order to calculate the profile of electric intensity field generated at the resonance. Obtained results presented in Fig. 2b reveal that the LRSP evanescent field probes the sensor surface with a penetration depth of $L_p=550$ nm (defined as the distance from the surface into the adjacent sample at which the amplitude the evanescent field drops to $1/e$). This value is about three-fold higher than $L_p=181$ nm of regular SPs. From the shift of the resonance in reflectivity spectra $R(\theta)$ associated with the immobilization of IgG antibody recognition elements shown in Fig. 2a, surface mass density of attached IgG molecules of $\Gamma=3.43\pm0.96$ ng mm^{-2} was determined (error represents chip-to-chip standard deviation). This value is close to that of a packed

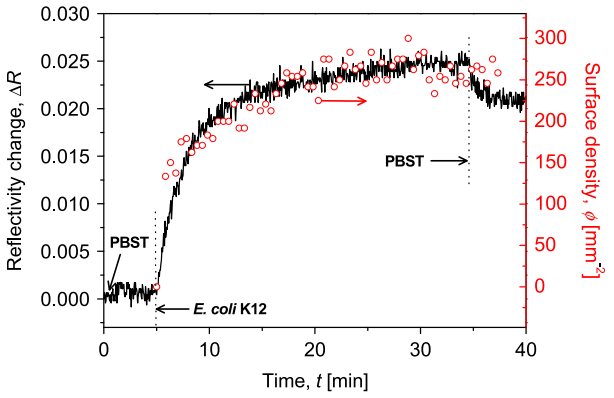

Fig. 3. Simultaneous observation of affinity binding of *Escherichia coli* K12 by SPR (sensor response ΔR) and optical microscopy (determined surface density). Analyte was dissolved in PBST at a concentration of 10^8 cfu mL^{-1} and flowed with the flow velocity of $v_{max}=8.8$ mm s^{-1}.

monolayer [27] and it translates to the distance between attached molecules comparable to size of IgG molecules (hydrodynamic radius of around 5.5 nm).

3.2. Surface density of captured analyte

Firstly, a PBST sample with *E. coli* K12 dissolved at a concentration of $c=10^8$ cfu mL^{-1} was flowed over the surface that was functionalized by specific p-IgG antibody. The flow velocity was set to $v_{max}=8.8$ mm s^{-1} and after 30-min flow of a sample the sensor surface was rinsed with PBST for 5 min. The binding of *E. coli* K12 was simultaneously observed by the SPR sensor with LRSP-supporting architecture and by using an optical microscope. As respective kinetics in Fig. 3 show, the equilibrium in the SPR reflectivity signal $R(t)$ was reached after ~20 min when the reflectivity change reached $\Delta R=0.025\pm8\times10^{-4}$ (error represents the standard deviation). The parallel optical microscopy measurements revealed that such SPR change corresponds to the surface density of adhered cells of $\phi=250\pm15$ cells mm^{-2} (error represents the standard deviation). For the average diameter of *E. coli* K12 of $a=1.54$ μm, these data indicate that the surface coverage of bacteria was ~0.05% that is consistent with observations reported by other groups [28–30]. Assuming that the sensor response ΔR is proportional to the number of cells on the surface ϕ, the minimum number of adhered cells that can be detected by the SPR sensor can be estimated as $3\phi\sigma_R/\Delta R$. The obtained data indicate that the SPR biosensor with LRSP layer architecture is capable to detect ~24 cells mm^{-2}. In the initial stage of the binding, the concentration of the analyte on the surface is negligible. Then, the flux of cells diffusing to the surface can be estimated as the diffusion rate k_m (defined by equation [1]) that is multiplied by the concentration of *E. coli* K12 in a sample. For the used flow rate v_{max}, the diffusion rate of $k_m=1.27\times10^{-4}$ mm s^{-1} was calculated which corresponds to the flux of *E. coli* K12 of about 13 cells mm^{-2} s^{-1}. This value is an order of magnitude larger than measured affinity binding rate which yielded ~1 cell mm^{-2} s^{-1}. In general, these surface densities are very low and cannot be described as a growth of a compact layer on the surface of which refractive index change is measured (which is typically assumed in classical SPR biosensors). Rather, measured variations in SPR reflectivity are associated with increased losses of probing LRSP waves occurring due to the scattering on sparsely distributed adhered cells.

3.3. Flow-rate dependence

Afterwards, the affinity binding experiment was repeated for the sample flow velocity varied between $v_{max}=2.2$ and

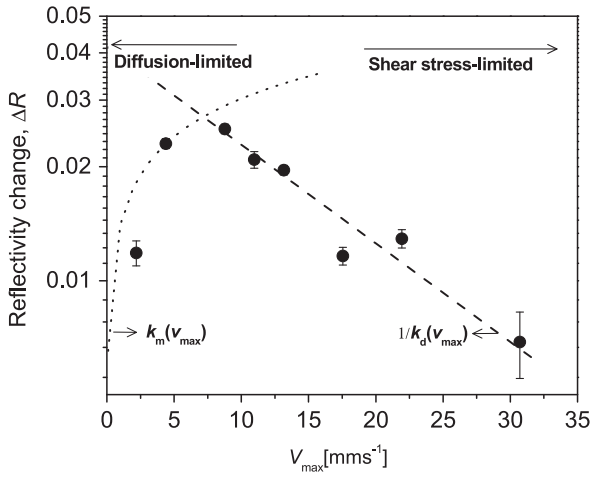

Fig. 4. Dependence of SPR sensor response ΔR on the flow velocity v_{max}. The concentration of *E. coli* K12 in PBST was of 10^8 cfu mL^{-1} and the affinity binding to specific antibodies p-IgG on the surface probed by LRSPs.

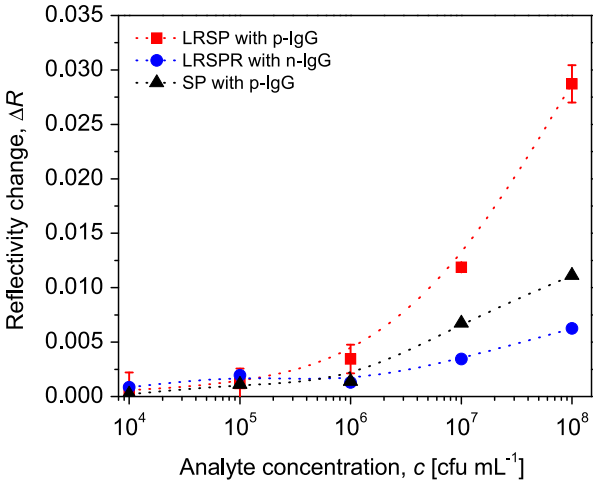

Fig. 5. Calibration curves measured for the detection of *E. coli* K12 by using sensor chips supporting LRSPs and regular SPs. Samples were flowed over surfaces modified with p-IgG specific to *E. coli* K12 epitopes on surface architectures supporting LRSP (solid squares) and SP (solid triangles). In addition, control experiment with reference n-IgG (against *E. coli* O157:H7) on the surface supporting LRSP is presented (solid circles).

30.7 mm s^{-1} (all other parameters were kept identical as in the previous Section 3.2). The obtained dependence of the saturation reflectivity change ΔR on the v_{max} is plotted in Fig. 4. It shows that ΔR increases with the flow rate v_{max} below 8 mm s^{-1}. The response ΔR peaks around this value and when further increasing v_{max} the sensor response ΔR rapidly decreases. For low flow rate $v_{max} < 8$ mm s^{-1}, the sensor is in "diffusion-limited" regime and the density of captured cells ϕ increases with v_{max} as the diffusion mass transfer rate k_m is proportional to $v_{max}^{1/3}$ (see Eq. (1)). However, when the flow rate is large $v_{max} > 8$ mm s^{-1}, the sensor is in "shear force-limited" regime and the sensor response exponentially decreases with v_{max}. In this regime, the measured dependence agrees with the analytical formula presented in Eq. (3) assuming that the equilibrium surface mass density is inversely proportional to k_d. From Eq. (2) follows that adhered *E. coli* K12 were exposed to a drag force between $F_d = 1.8$ pN ($v_{max} = 2.2$ mm s^{-1}) and 25 pN ($v_{max} = 30.7$ mm s^{-1}) which is in the range of forces that were reported for protein interactions [31].

3.4. Effect of probing depth

The strength of sensor response ΔR induced by the binding of bacterial analyte was compared for SPR biosensor architectures supporting LRSP and regular SP waves. The analyte *E. coli* K12 was dissolved at concentrations between $c = 10^4$ and 10^8 cfu mL^{-1} in a series of samples that were successively flowed over the sensor surface. Each sample was incubated for 20 min followed by the rinsing with PBST for 20 min. The flow velocity of $v_{max} = 8.8$ mm s^{-1} was used as it provides largest sensor response ΔR (see Section 3.3). Fig. 5 shows measured calibration curves for *E. coli* K12 samples flowed over the sensor surface with immobilized specific antibodies (p-IgG against *E. coli* K12, target) and reference antibodies (n-IgG against *E. coli* O157:H7, reference). One can see that the specific response on LRSP-supporting sensor chip is around three times larger than that measured with regular SPs. This improvement is comparable to the figure of merit enhancement by a factor of four [24] and it is similar to that reported by Vala et al. [19]. The control experiment reveals that on the surface with reference antibodies n-IgG (not specific to the target analyte) the amount of captured *E. coli* K12 cells was five times lower compared to that carrying specific antibodies p-IgG. Let us note that identical architecture was used in our previous studies for an LRSP-based immunoassay detection of other analytes (*E. coli* O157:H7) with excellent specificity [18,21]. In addition, LRSPs were utilized for the analysis of real samples such as milk and serum based on similar thiol SAMs [32] and zwitterionic polymer coatings [20].

4. Conclusions

The paper demonstrates the importance of precise control of flow conditions and optimization of surface plasmon probing depth in SPR biosensors for detection of large bacterial pathogen analytes. Firstly, achieved results reveal that of a balance between the analyte mass transfer rate and stability of affinity bound analyte to the surface occurs in a very narrow window of flow velocities. The observed "diffusion-limited" and "shear stress-limited" regimes were in accordance with other works reported on protein interactions and qualitatively agreed with presented analytical theory. Secondly, we show that the probing of the sensor surface by surface plasmon waves with the probing depth matching to the size of target analyte allows to significantly enhance the sensor response. In particular, the using of long range surface plasmons improved the sensitivity for detection of model *E. coli* analyte by factor of three when compared to regular SPs. Moreover, the presented work also provides leads for the optimization of other types of SPR-based biosensors developed in our and other laboratories for the analysis of bacterial pathogens. These include biosensors relying on surface plasmon-enhanced fluorescence spectroscopy [21] and SPR biosensor with magnetic nanoparticle-enhanced assays [18] as well as those relying on phage recognition elements which exhibit order of magnitude larger size than most commonly used antibodies [33,34].

Acknowledgment

We thank Marlies Czetina (Bioresources business unit at Health and Environment Department, AIT) for preparation of *E. coli K*12 samples. This work was partially supported by the Austrian NANO Initiative (FFG and BMVIT) through the NILPlasmonics project within the NILAustria cluster (www.NILAustria.at), Austrian Science Fund (FWF) through the project ACTIPLAS (P 244920-N20), and by Taiwanese National Science Council (NSC-102-2221-E-008-011).

References

[1] J. Homola, Chem. Rev. 108 (2008) 462–493.
[2] K.S. Gracias, J.L. McKillip, Can. J. Microbiol. 50 (2004) 883.
[3] S. Yaron, K.R. Matthews, J. of Appl. Microbiol. 92 (2002) 633–640.
[4] A.D. Taylor, Q.M. Yu, S.F. Chen, J. Homola, S.Y. Jiang, Sens. Actuators B 107 (2005) 202–208.
[5] B.K. Oh, W. Lee, W.H. Lee, J.W. Choi, Biotechnol. Bioprocess Eng. 8 (2003) 227–232.
[6] P.M. Fratamico, T.P. Strobaugh, M.B. Medina, A.G. Gehring, Biotechnol. Tech. 12 (1998) 571–576.
[7] V. Koubova, E. Brynda, L. Karasova, J. Skvor, J. Homola, J. Dostalek, P. Tobiska, J. Rosicky, Sens. Actuators B 74 (2001) 100–105.
[8] A.D. Taylor, J. Ladd, Q.M. Yu, S.F. Chen, J. Homola, S.Y. Jiang, Biosens. Bioelectron. 22 (2006) 752–758.
[9] O. Tokarskyy, D.L. Marshall, Food Microbiol. 25 (2008) 1–12.
[10] S.C. Kuo, D.A. Hammer, D.A. Lauffenburger, Biophys. J. 73 (1997) 517–531.
[11] Z.J. Li, N. Mohamed, J.M. Ross, Biotechnol. Prog. 16 (2000) 1086–1090.
[12] C. Verdier, C. Couzon, A. Duperray, P. Singh, J. Math. Biol. 58 (2009) 235–259.
[13] M.D. Zordan, M.M.G. Grafton, G. Acharya, L.M. Reece, C.L. Cooper, A.I. Aronson, K. Park, J.F. Leary, Cytom. Part A 75A (2009) 155–162.
[14] A. Ghubade, S. Mandal, R. Chaudhury, R.K. Singh, S. Bhattacharya, Biomed. Microdevices 11 (2009) 987–995.
[15] L.J. Yang, Talanta 80 (2009) 551–558.
[16] E. de Boer, R.R. Beumer, Int. J. Food Microbiol. 50 (1999) 119–130.
[17] A.E. Balaev, K.N. Dvoretski, V.A. Doubrovski, in: V.V. Tuchin (Ed.), Saratov Fall Meeting 2001: Optical Technologies in Biophysics and Medicine III, SPIE-International Society for Optical Engineering, Bellingham, 2001, pp. 253–260.
[18] Y. Wang, W. Knoll, J. Dostalek, Anal. Chem. 84 (2012) 8345–8350.
[19] M. Vala, S. Etheridge, J.A. Roach, J. Homola, Sens. Actuators B 139 (2009) 59–63.
[20] C.J. Huang, L. Mi, S.Y. Jiang, Biomaterials 33 (2012) 3626–3631.
[21] C.J. Huang, A. Sessitsch, J. Dostalek, W. Knoll, Anal. Chem. 83 (2011) 674–677.
[22] R. Mejard, J. Dostalek, C. Huang, H. Griesser, B. Thierry, Opt. Mater. 35 (2013) 2507–2513.
[23] S. Slavik, J. Homola, Sens. Actuators B 123 (2007) 10–12.
[24] J. Dostalek, A. Kasry, W. Knoll, Plasmonics 2 (2007) 97–106.
[25] C.J. Huang, J. Dostalek, W. Knoll, J. of Vac. Sci. Technol. B 28 (2010) 66–72.
[26] D.A. Edwards, Bull. Math. Biol. 63 (2001) 301–327.
[27] C. Vollenkle, S. Weigert, N. Ilk, E. Egelseer, V. Weber, F. Loth, D. Falkenhagen, U.B. Sleytr, M. Sara, Appl. Environ. Microbiol. 70 (2004) 1514–1521.
[28] A.G. Gehring, D.M. Albin, A.K. Bhunia, S.A. Reed, S.I. Tu, J. Uknalis, Anal. Chem. 78 (2006) 6601–6607.
[29] J.M. Simpson-Stroot, E.A. Kearns, P.G. Stroot, S. Magana, D.V. Lim, J. Microbiol. Methods 72 (2008) 29–37.
[30] J.D. Brewster, A.G. Gehring, R.S. Mazenko, L.J. VanHouten, C.J. Crawford, Anal. Chem. 68 (1996) 4153–4159.
[31] M. Strigl, D.A. Simson, C.M. Kacher, R. Merkel, Langmuir 15 (1999) 7316–7324.
[32] Y. Wang, A. Brunsen, U. Jonas, J. Dostalek, W. Knoll, Anal. Chem. 81 (2009) 9625–9632.
[33] L. Gervals, M. Gel, B. Allain, M. Tolba, L. Brovko, M. Zourob, R. Mandeville, M. Griffiths, S. Evoy, Sens. Actuators B 125 (2007) 615–621.
[34] M. Mejri, H. Baccar, E. Baldrich, F. Del Campo, S. Helali, T. Ktari, A. Simonian, M. Aouni, A. Abdelghani, Biosens. Bioelectron. 26 (2010) 1261–1267.